Experimental Study of the Flow Structure Including Whirlwinds in the Wake Region of a Flame in a Cross-wind

Masahiko Shinohara[1] and Kazuhiko Kudo[2]

[1]*National Research Institute of Fire and Disaster, 14-1 Nakahara 3-Chome, Mitaka, Tokyo 181-8633, Japan*
[2] *Division of Mechanical Science, Hokkaido University, Kita-13 Nishi-8, Kita-ku, Sapporo 060-8628, Japan*

Abstract

The flow structure of whirlwinds and the near field in the downwind side of a methanol flame was experimentally studied with flow visualization. It is shown that whirlwinds in the downwind side of a flame start from the velocity boundary layer on a floor and flow to the downwind direction extending upwards. Whirlwinds are pairs of alternating counter-rotating periodical vortices. Some origins and formations of whirlwinds are discussed. Moreover, We observed: a V-shaped area, where a cross-wind does not enter inside, in the downwind side of the flame on the floor level; two reverse flows, which flow towards the flame along the inner boundaries of the V-shaped area; and a wall vortex pair which extends from the end of the flame on the floor under the counter-rotating vortex pair within the plume from the flame deflected by a cross-wind. The wall vortex pair was investigated by particle image velocimetry (PIV).

1. Introduction

Whirlwinds and fire whirls have caused destructive damage in large scale fire incidents such as city fires and forest fires. Whirlwinds are intense atmospheric tornado-like vortices; fire whirls are whirlwinds contain fire in themselves. In the Kanto Earthquake of 1923 in Japan, 38,000 people lost their lives by fire whirls.

In order to develop measures against whirlwinds and fire whirls in fire incidents, we have to understand the mechanisms and the conditions for formation of whirlwinds and fire whirls. Church et al [1] observed three types of vortices in a large thermal plume in an outdoor experiment using 105 fuel-oil burners with a total output of around 1000 MW, and proposed mechanisms of such vortices production. Terada [2], Fujiwara [3] and Soma [4]

Corresponding Author- Tel.: +81-422-44-8364;
Fax: +81-422-44-8364
E-mail address: shino@fri.go.jp

proposed mechanisms for fire whirl in the Kanto Earthquake of 1923 in Japan. However, these mechanisms proposed by these researchers have not been proved. Soma and Saito [5] confirmed that three types of fire whirls were formed in experiments which satisfy scaling laws for each types proposed by them. However, the reason why fire whirls occur on such conditions was not made clear.

This study was performed in order to understand the mechanism of formation of whirlwinds in the downwind side of fire area. This type of whirlwinds is the most reported type of whirlwinds occurred in fire incidents [6]. In addition, a flow issuing perpendicularly into a cross-wind is a basic and an important flow configuration found in the atmosphere, ocean and many engineering applications; in case of whirlwinds in the downwind side of fire area, the flow is the plume from fire. In case that the flow is a jet, jet in cross-wind has been widely studied by many researchers [7].

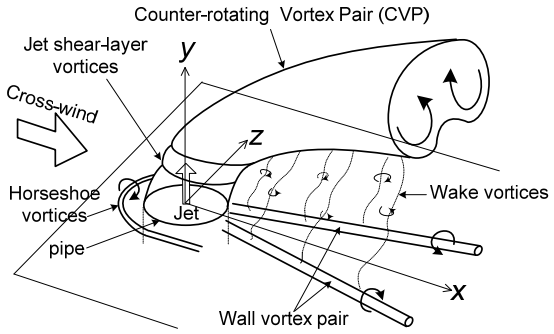

Fig.1 Schematic of the vortical structure associated with a jet in a cross-wind. This figure is the combination of figures in Fric and Roshko[8] and Keslo et.al.[9] and modified.

We explain the flow structure in the downwind side of a flame by comparing with the flow structure in the downwind side of a jet. It has been reported that there are five vortical systems associated with a jet in cross-wind. They are illustrated in Fig.1, which is the combination of figures in [8] and [9] and modified. They are 'wake vortices', 'wall vortex pair', 'Counter-rotating vortex pair (CVP)', 'jet shear-layer vortices' and 'horseshoe vortices'.

Frick and Roshko [8] found that 'wake vortices have their origins in the laminar boundary layer on the wall from which the jet issues'. In case of fire in cross-wind, wake vortices in the downwind side of fire are called 'whirlwinds' in the remainder of this paper. Whirlwinds have been also observed in the downwind side of fire in large scale fire incidents and some experiments [1, 5, 10-12]. Fig.2 is the schematic of the flow around the flame in cross-wind consisting of the flow which has been reported until now and the flow which was found in this work. We discussed the structure, origin and formation of whirlwinds in the downwind side of a flame in §3.2 by comparing with those of vortices shedding from a solid bluff body and wake vortices behind a jet in a cross-wind.

The wall vortex pair, which lie on the

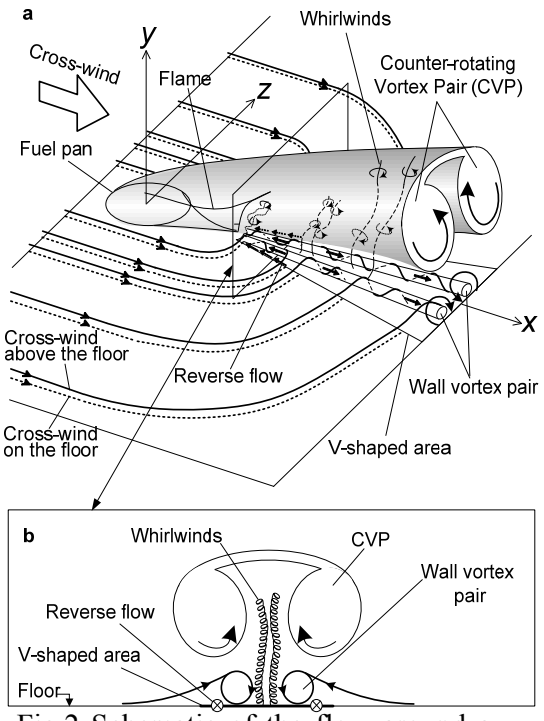

Fig.2 Schematic of the flow around a flame in a cross-wind.

floor in the downwind side of a jet, has been studied by only a few researchers (9, 13). We found that there is the wall vortex pair in the downwind side of a flame as well (Fig.2). The structure investigated with flow visualization and particle image velocimetry (PIV) is described in §3.3.3.

The CVP has been reported in the plume from fire deflected by the cross-wind [14] as well as in the downwind side of a jet [15, 16]. The CVP was not paid attention in our experiment, but some results of the CVP associated with the wall vortex pair are shown in §3.3.3.

Horseshoe vortices were not observed around the flame in cross-wind in our experimental condition.

2. Experimental Apparatus and Method

The experiments were carried out using an open low-speed wind tunnel with the working section of 400 mm square cross section and 800 mm long (Fig.3). The cross-wind has a velocity U ranging from 0.14 to 0.79 ms^{-1}. The fuel pool with an inner diameter D of 30 mm or 80 mm was placed flush with the tunnel floor. The level of methanol used as the fuel was adjusted to be at the floor level throughout the experiments. Airflow structure around the methanol flame was investigated with flow visualization by smoke wire or a sheet of laser light and particle image velocimetry (PIV).

The velocity field in yz plane was obtained using PIV. The PIV illumination source is Nd: YAG laser (New wave research Solo II, 30 mJ/pulse at 532 nm wavelength, 10 Hz double-pulse repetition frequencies). A cylindrical lens (15mm focal length) spreads the laser beam into a sheet to illuminate a planar section of the flow field. A CCD camera (Kodak ES 1.0, 1008 × 1018 pixel) with zoom lens (Nikkor, 28-85mm focal length, f/2.8) captured the light scattered from the seeding particles in laser sheet. Velocity fields were obtained with cross-correlation method. In the remainder of this paper, the velocity boundary layer on the floor is called 'the floor boundary layer'.

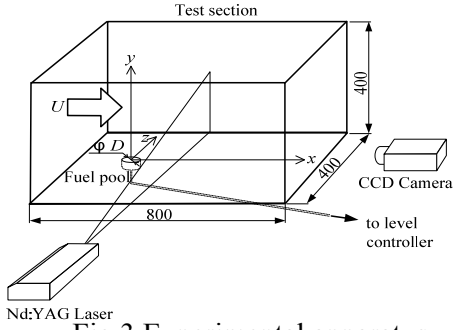

Fig.3 Experimental apparatus.

3. Results

3.1 Flow structure in the downwind side of a flame

Airflow patterns around the flame in cross-wind from 0.14 to 0.79 ms^{-1} were visualized by streak line generated by smoke wire placed at the right angle of the cross-wind and parallel to the floor at the upwind side of the flame. Figure 4-1 ~ 4-3 show representative cross-sectional views for different velocity of cross-wind U = 0.24, 0.32 and 0.56 ms^{-1} respectively. Each figure consists of 4 photographs in which smoke wire is placed at different height h from the floor. In each photograph, the cross-wind direction is from left to right. The circle of the left-hand side of each photograph is the fuel pool. Flame rises and extends to downwind direction from the pool. Smoke lines in each photograph show that the cross-wind around the flame above the floor level converges at the downwind side of the flame after the cross-wind goes past the side of the flame. It is most likely caused by air entrainment into the flame. In the remainder of this paper,

we describe whirlwinds and other airflow structures.

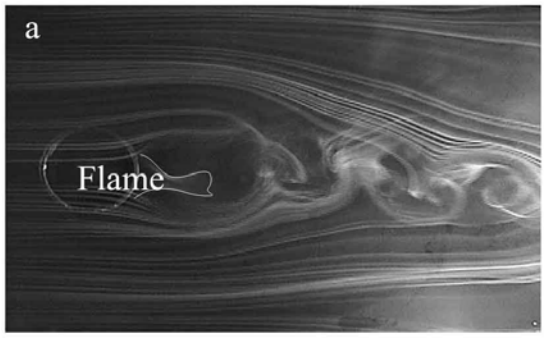

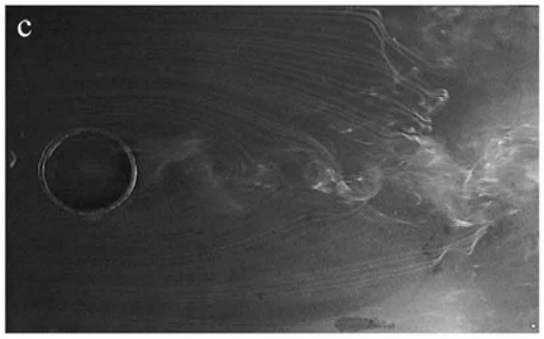

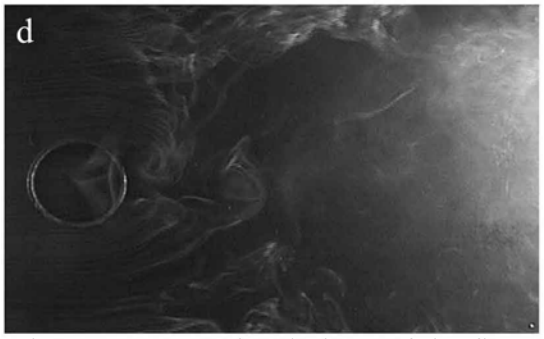

Fig.4-1 Cross-sectional views of the flow around the flame in U = 0.24ms^{-1}. D = 80mm. Smoke come from different height: a)$h = D$; b) $h = D/2$; c) $h = D/8$; d) $h = 0+\delta$.

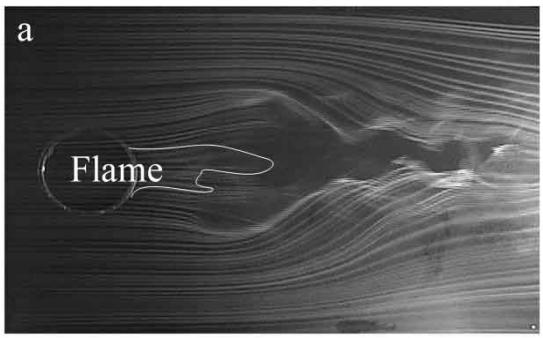

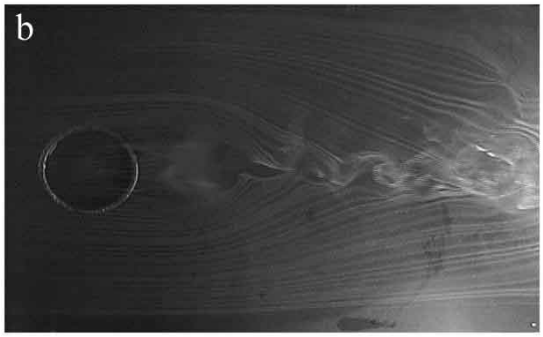

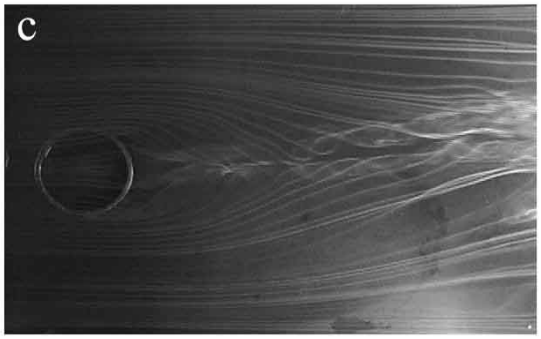

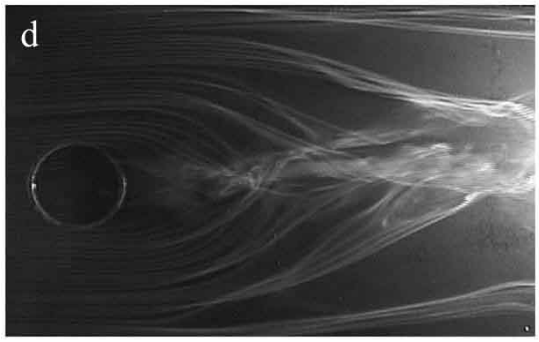

Fig.4-2 Cross-sectional views of the flow around the flame in U = 0.32ms^{-1}. D = 80mm. Smoke comes from different height: a)$h = D$; b) $h = D/2$; c) $h = D/8$; d) $h = 0+\delta$.

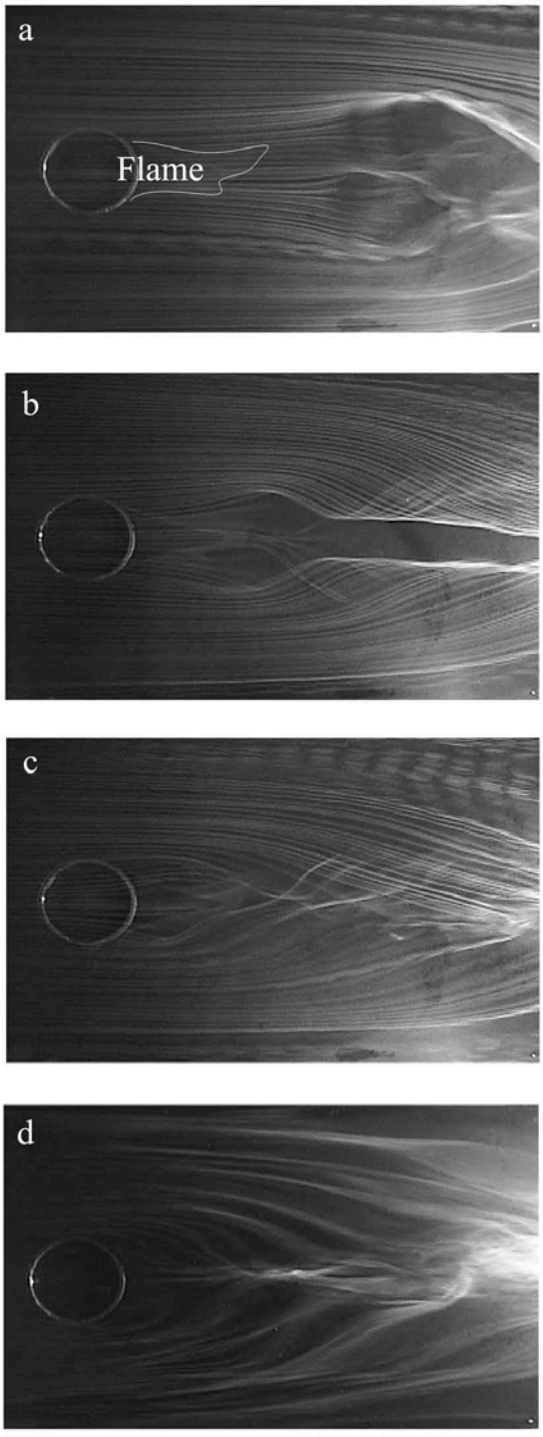

Fig.4-3 Cross-sectional views of the flow around the flame in U = 0.56ms^{-1}. D = 80mm. Smoke comes from different height: a)$h = D$; b) $h = D/2$; c) $h = D/8$; d) $h = 0+\delta$.

3.2 Whirlwinds in the downwind side of a flame

3.2.1 Structure of whirlwinds

Fig.5 is a cross-sectional view of whirlwinds in the downwind side of the flame. Smoke seeded into the cross-wind is illuminated by a sheet of laser light, which is set parallel to the floor at the height of 40 mm from the floor. The photograph shows that whirlwinds in the downwind side of the flame are pairs of alternating counter-rotating periodical vortices similar to Kármán vortex shedding from a solid bluff body.

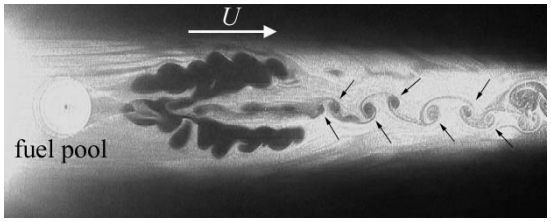

Fig.5 Cross-sectional view of whirlwinds for U = 0.49ms^{-1}. D = 80mm.

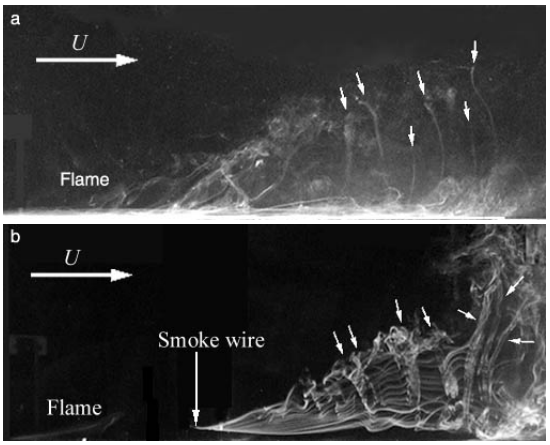

Fig.6 Side views of whirlwinds for U = 0.46m s^{-1}. D = 80mm. a) A smoke wire is set at the height just above the floor at the upwind side of the flame. b)It is set at 20 mm parallel to the floor at the downwind side of the flame.

However, we found out that whirlwinds start from the floor boundary layer in the downwind side of the flame at $U \geq 0.24$ ms^{-1}. It is different in origin from Kármán vortex shedding from a solid bluff body. Fig.6a and Fig.6b are side

views of whirlwinds in the downwind side of the flame in the cross-wind (U = 0.46 ms^{-1}). In Fig.6a, smoke wire is placed at the height just above the floor in the floor boundary layer at the upwind side of the flame. The figure shows that whirlwinds start from the floor boundary layer at the downwind side of the flame and flow to the downwind direction extending upwards. This formation of whirlwinds is same as that of wake vortices behind a jet in a cross-wind [8]. When smoke wire was placed at 20 mm parallel to the floor at the downwind side of the flame, we can only see whirlwinds at height above 20 mm in the downstream of the smoke wire, but not below 20 mm (Fig. 6b). This photograph shows more clearly that whirlwinds extend upwards.

3.2.2 Vorticity source and formation of whirlwinds

In this chapter, vorticity source and formation of whirlwinds are discussed. In §3.2.1, we explained that whirlwinds originate in the floor boundary layer. We observed the flow around the flame in the floor boundary layer carefully in order to understand the vorticity source and formation of whirlwinds.

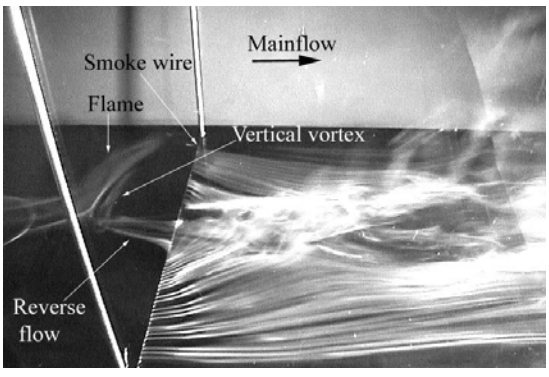

Fig.7 Formation of a vertical vortex from reverse flows. U = 0.46ms^{-1}. D = 80mm.

We observed that two reverse flows and cross-wind combine and form a vertical vortex. 'Reverse flows' flow towards the flame against cross-wind in the downwind side of the flame. They are described in §3.3.2 and drawn in Fig.2 as well. Fig.7 is a diagonal view of reverse flows in the downwind side of the flame for U = 0.46 ms^{-1}. The smoke wire is placed at the right angle of the cross-wind and parallel to the floor at the downwind side of the flame at the height just above the floor. This figure shows that two reverse flows turn to upward direction and become a vertical vortex at the just downwind side of the flame. Fig.8 is a diagonal view at the just downwind side of the flame for U = 0.46 ms^{-1}. The smoke is injected into only this half side at the floor height. Cross-wind which turned around the flame on the floor and a reverse flow combine and form a vertical vortex at just downwind side of the flame.

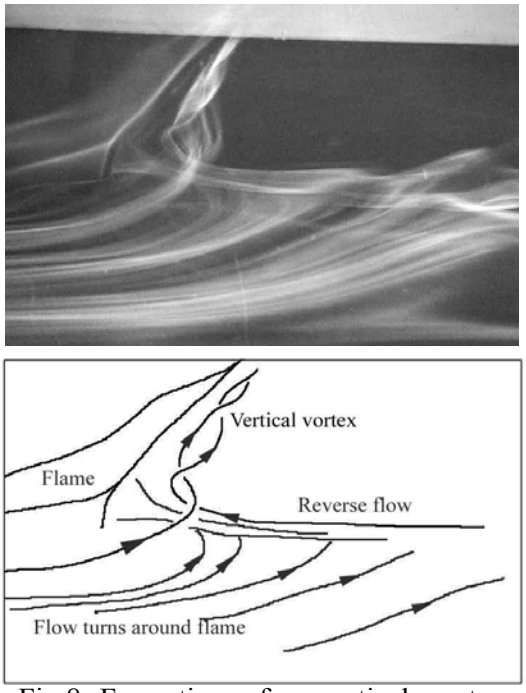

Fig.8 Formation of a vertical vortex from a reverse flow and a cross-wind. U = 0.46m s^{-1}. D = 80mm.

Furthermore, Fig.9 is a diagonal view of two steady-state vortex pair at just downwind side of the flame viewing from the end of the flow. The right vortex turns in clockwise direction, and the left one turns in counter-clockwise direction. The

figure shows that the vortex pair is formed by cross-wind turned around the flame on the floor. The vertical vortex in Fig.7 and Fig.8 seems to be one of the vortex pair in Fig.9.

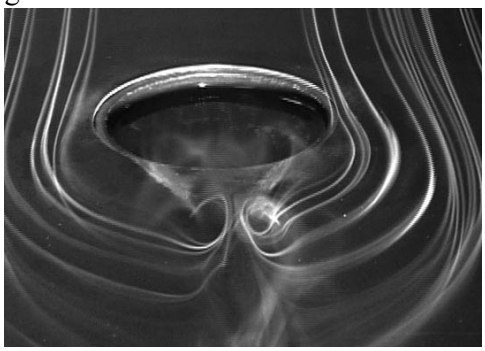

Fig.9 Formation of a vertical vortex from cross-wind. $U = 0.46\text{m s}^{-1}$. $D = 80\text{mm}$.

The vertical vortex in Fig.7 and Fig.8 seems to be the beginning of whirlwinds. This phenomenon has not been reported as the beginning of the wake vortices behind a jet in a cross-wind. It suggests that the mechanism of formation of whirlwinds may be different from that of the wake of the jet originating from the separation of the boundary layer on the floor [8].

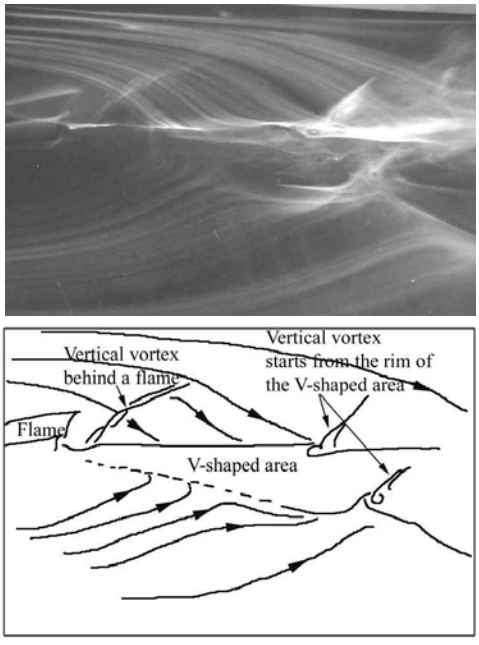

Fig.10 Formation of a vertical vortices at the rim of the V-shaped area. $U = 0.46\text{m s}^{-1}$. $D = 80\text{mm}$. $h = 0+\delta$.

Vertical vortices generated at other locations are shown in Fig.10. They start from the rim of the V-shaped area, where the cross-wind does not enter inside at the downwind side of the flame on the floor level. V-shaped area is described in §3.3.1 and drawn in Fig.2 as well. These vortices generated at these locations were observed for $U \geq 0.32\ \text{ms}^{-1}$.

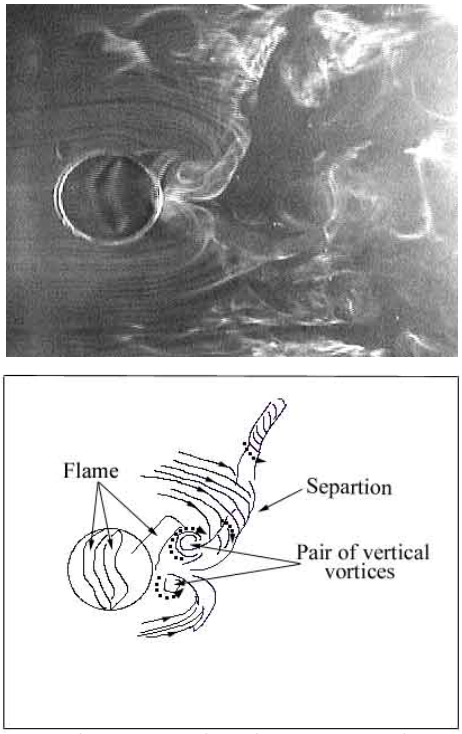

Fig.11 The separation is connected to the vertical vortex. $U = 0.24\text{ms}^{-1}$. $D = 80\text{mm}$.

For $U = 0.24\ \text{ms}^{-1}$, the separation of the flow in the floor boundary layer is connected to one of the pair of vertical vortices located at just downwind side of the flame (Fig.11). This phenomenon is the same as that observed in the wake of transverse jet [8]. The separation and the pair of vertical vortices occur at the almost same time. The interrelation between the separation and the pair of vertical vortices was not clear from the observation. Fric and Roshko [8] showed that roll-up after separation is entrained and convected by the jet, extended and becomes to be wake vortices. This suggests the interrelation

between the separation and the pair of vertical vortices at the downwind side of the flame. This type of formation of whirlwinds was not observed for $U \geq 0.32$ ms^{-1}.

3.2.3 Strouhal frequencies of whirlwinds

Strouhal frequency *St* was measured in order to compare whirlwinds in the downwind side of the flame with vortices in both the wake of a jet and the wake of a circular cylinder. *St* (= *fD*/*U*) for whirlwinds is based on frequency of whirlwinds *f*, the fuel-pool diameter *D* and the cross-wind velocity *U*. *St* for $U = 0.24$ ms^{-1} ($Re = UD/\nu = 1300$) was 0.8 ~ 1.3 and *St* for $U = 0.46$ ms^{-1} ($Re = 2430$) was 1.15 ~ 1.55. This value is larger than 0.21 for the wake of a circular cylinder for the same *Re*. *St* for a jet wake for same *Re* is not known, but *St* for $Re = 3800 \sim 11400$ is 0.07 ~ 0.20 [8]. The large *St* of whirlwinds may also suggest that the formation mechanisms of whirlwinds are different from those of vortices in both the wake of a jet and the wake of a circular cylinder.

3.3 Flow structure near the floor in the downwind side of a flame

In this section, three types of airflow structure near the floor in the downwind side of the flame are described. We found these flow structures when we visualized the flow near the floor around the flame in order to investigate the formation of whirlwinds.

3.3.1 V-shaped area

There is a long V-shaped area, where the cross-wind does not enter inside, in the downwind side of the flame on the floor level. Fig.12a-f show top views of the V-shaped area. The smoke wire is placed at the right angle of the cross-wind at the floor level at the upwind side of the flame. The V-shaped area was not observed for $U < 0.26$ ms^{-1}. The angle of the V-shaped area α decreases with increasing cross-wind velocity *U*. These correlations can be expressed as $\alpha = 13.68U^{-0.72}$ when $U =$ 0.26 - 0.79 ms^{-1}.

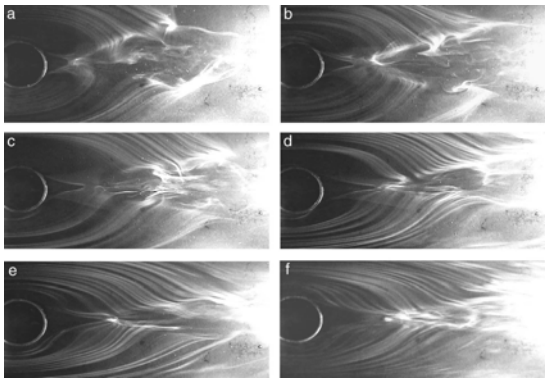

Fig.12 Top views of V-shaped area. a) $U = 0.26$ ms^{-1}; b) $U = 0.32$ ms^{-1}; c) $U = 0.46$ ms^{-1}; d) $U = 0.56$ ms^{-1}; e) $U = 0.67$ ms^{-1}; f) $U = 0.79$ ms^{-1}.

3.3.2 Reverse flow

In order to observe the flow structure in the V-shaped area, we set a smoke wire in the V-shaped area on the floor. Fig.13 shows that there are two reverse flows, which flow towards the flame on the floor level. Reverse flows exist at $x \leq 2.5D$ (Fig.13a-c), however no reverse flow exists at $x > 2.5D$ (Fig.13d), when $U = 0.46$ ms^{-1}. Reverse flows are same as the flow shown in Fig.7. These flows are at the inner boundaries of the V-shaped area on the floor level.

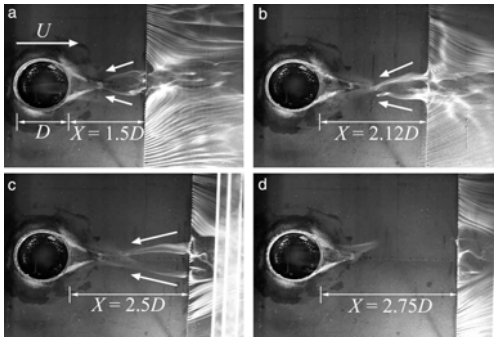

Fig.13 Top views of two reverse flows. $D = 80$mm. $U = 0.46$m.

3.3.3 Wall vortex pair

We found a wall vortex pair, which lies on the floor from the end of the flame at a velocity of $U \geq 0.32$ ms^{-1} for D = 80mm (Fig.4) and at $U \geq 0.14$ ms^{-1} for D = 30mm. Fig.14 shows the top view of the airflow around the flame in the floor boundary layer in cross-wind (U = 0.46 ms $^{-1}$). With the wind from the wind tunnel, the flame deflected and has a triangular region where it touches the floor locating beside the rim of the pool. The wall vortex pair shown by arrows in Fig.14 extends from the tip of the triangular region, where the flame does not touch the floor anymore, at the downwind side of the flame on the floor within the floor boundary layer.

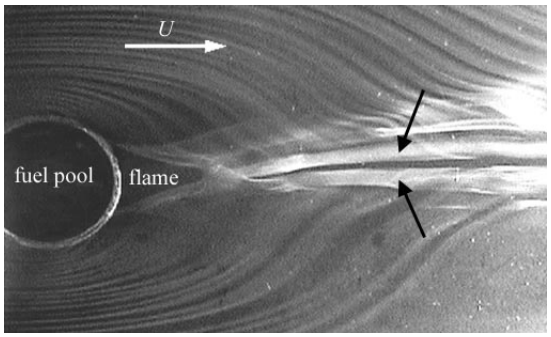

Fig.14 Top view of the wall vortex pair, which is shown by arrows. A smoke wire is placed at 5 mm parallel to the floor. D=80mm. U=0.46ms^{-1}.

A view from the end of the flow

Fig.15 View from the end of the wall vortex pair of fig14.

(Fig.15) shows that the converging cross-wind on both side flow towards each other, rise gradually and form the wall vortex pair (Fig.2). The wall vortex pair is composed of two vortices turning in a direction opposite to each other. The right vortex turns in counter-clockwise direction, and the left one turns in clockwise direction. Both of the vortices of the wall vortex pair have two sections that flow in opposite direction. Vortex near the flame flows towards the flame, whereas the rest of the section flows to the downwind direction (Fig.2). Sometimes the downwind part of a vortex of the wall vortex pair rises obliquely and becomes a vertical vortex.

Fig.16 shows that the wall vortex pair is located under the counter-rotating vortex pair (CVP). Fig.16a is the photograph taken from the end of the flow for U = 0.55 ms^{-1} and D = 30 mm. Smoke seeded into cross-wind is illuminated by a sheet of laser light, which is set vertical to the cross-wind at x = 6.5 D. This photograph shows that each vortex of the wall vortex pair converges at its center. Fig.16b is projected instantaneous velocity vectors in yz plane at x = 6.5 D for U = 0.55 ms^{-1} and D = 30mm. This figure shows that the wall vortex pair rotates in the reverse direction to the CVP. Flows going to xy plane diverge in two directions: one goes upward and another goes downward.

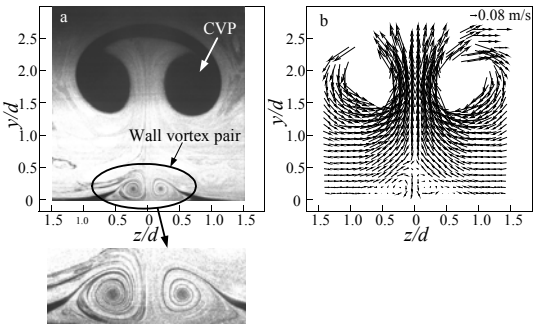

Fig.16 a) Vertical sectional view at x =6.5 D from the downwind direction for U = 0.55ms^{-1}. D = 30mm. b) Projected velocity vectors in yz plane at x = 6.5 D for U = 0.55ms^{-1}. D = 30mm.

Fig.17 shows a representative set of projected instantaneous velocity vectors in yz planes at a) x = 3.5 D, b) x = 6.5 D and c) x = 9.5 D for U = 0.55 ms^{-1}. The location of x = 3.5 D is at approximately 25mm downwind side of the tip of the triangular region where the deflected flame

touches the floor for U = 0.55 ms^{-1}. The distance between vortices increases with

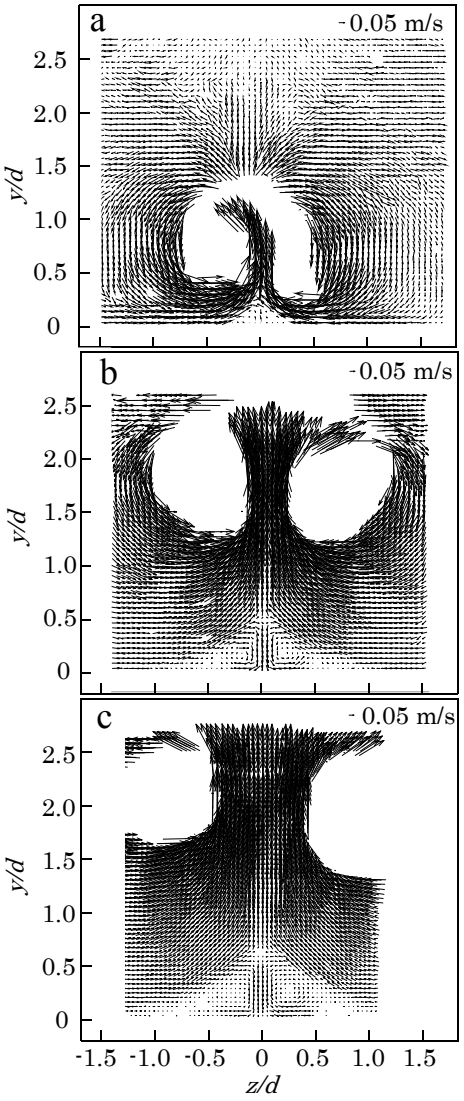

Fig.17 Projected velocity vectors in *yz* planes at a) x = 3.5d, b) x = 6.5d and c) x = 9.5d for U = 0.55ms^{-1}. D = 30mm.

increasing downstream distance x for both the wall vortex pair and the CVP. The diameter of the wall vortex increases with increasing downstream distance x. The height where flows diverge upward and downward increases with increasing downstream distance x. Fig.18 shows the distribution of the tangential velocity v at the height of the center of each wall vortex in 3 *yz* planes at x = 3.5 D, 6.5 D and 9.5D for U = 0.55 ms^{-1}. The center part of each vortex rotates as a rigid body; this part is shown by dotted lines with arrow in Fig.18. Fig.19 shows the variation of the tangential velocity gradient $|\partial v/\partial z|$ of the part rotates as rigid body at the height of the center of the wall vortices for U = 0.55 ms^{-1}. The tangential velocity gradients of the part between vortices shown by open circles and open triangles decrease with increasing downstream distance x, and are larger than those of the outside part of vortices shown

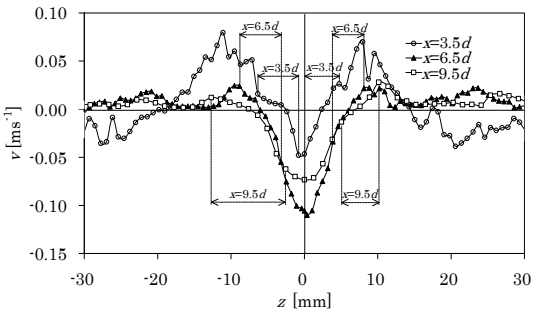

Fig.18 The distribution of the tangential velocity v in *yz* plane at x = 3.5D, 6.5D and 9.5D at the height of the center of each wall vortex for U = 0.55ms^{-1}.

by closed circles and closed triangles.

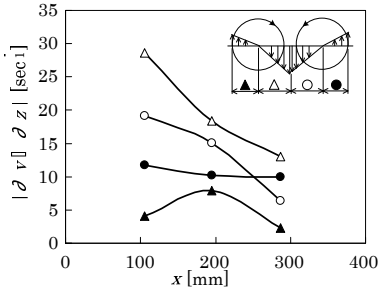

Fig.19 Variation of $|\partial v/\partial z|$ at the height of the center of each wall vortex for U = 0.55ms^{-1} with x.

Fig.20 show representative sets of projected instantaneous velocity vectors at yz plane at x = 6.5 D for a) U = 0.19 ms^{-1}, b) U = 0.42 ms^{-1} and c) U = 0.64 ms^{-1}. The diameter of the wall vortex decreases with increasing cross-wind velocity. The height where flows diverge upward and downward decreases with increasing cross-

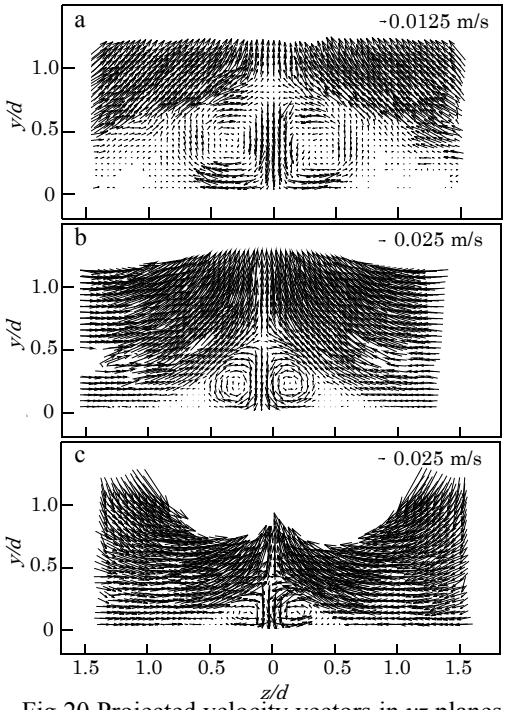

Fig.20 Projected velocity vectors in *yz* planes at $x = 6.5D$. D = 30mm. a) U = 0.19ms^{-1}; b) U =0.42ms^{-1};c) U =0.64ms^{-1}.

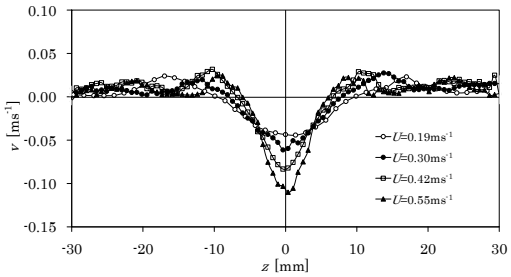

Fig.21 The distribution of the tangential velocity on *yz* plane at $x = 6.5d$ at the height of the center of the wall vortices for four cross-wind velocities.

wind velocity. Fig.21 shows the distribution of the tangential velocity v at the height of the center of each wall vortex in *yz* planes at $x = 6.5\ D$ for $U = 0.19$, 0.30, 0.42 and 0.55 ms^{-1}. The downward velocity at the part between wall vortices increases with increasing cross-wind velocity. The distance between wall vortices decreases with increasing cross-wind velocity. Fig.22 shows the variation of the tangential velocity gradient $|\partial v/\partial z|$ of the part rotates as rigid body at the height of the center of the wall vortices at $x = 6.5\ D$. The tangential velocity gradients increase with increasing cross-wind velocity U. The tangential velocity gradients of the part between vortices shown by open circles and open triangles are larger than those of the outside part of vortices shown by closed circles and closed triangles.

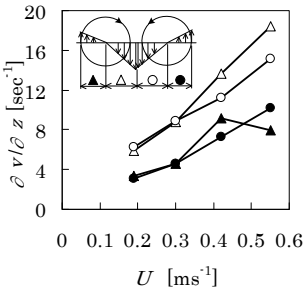

Fig.22 Variation of $|\partial v/\partial z|$ at the height of the center of each wall vortex at $x = 6.5D$

4. Conclusion

Whirlwinds in the downwind side of a flame are pairs of alternating counter-rotating periodical vortices similar to the structure of Kármán vortex street shedding from a solid bluff body. However, whirlwinds start from the velocity boundary layer on the floor and flow to the downwind direction extending upwards. This is different in origin and formation from the vortices shedding from a solid bluff body, whereas is the same as the wake vortices behind a jet in a cross-wind. Cross-wind which turned around the flame on the floor and reverse flows which flow towards the flame against cross-wind in the downwind side of the flame combine and form a vertical vortex at just downwind side of the flame. If this vertical vortex is the beginning of the whirlwinds, the mechanism of formation of whirlwinds may be different from that of the wake vortices of a jet in crosswind. For $U = 0.24$ ms^{-1}, the separation of the flow in the floor boundary layer is connected to one of the pair of vertical vortices located at just downwind side of the flame. This

phenomenon is similar to the beginning of wake vortices behind a jet in a cross-wind. Strouhal frequencies of whirlwinds in the downwind side of a flame are much larger than those of the vortices in the wake of a circular cylinder and a jet in a cross-wind.

There is a long V-shaped area, where the cross-wind does not enter inside, in the downwind side of the flame on the floor level. The angle of the V-shaped area decreases with increasing cross-wind velocity. Vertical vortices start from the rim of the V-shaped area as well as just downwind side of the flame. There are two reverse flows, which flow towards the flame along the inner boundaries of the V-shaped area on the floor level.

There is a wall vortex pair which lies on the floor under the CVP from the end of the flame. Wall vortices rotate in reverse direction to the CVP and their flows converge at each center. PIV measurements showed: 1) the diameter of the wall vortex and the distance between wall vortices increase with increasing downstream distance and decrease with increasing cross-wind velocity; 2) the tangential velocity gradients of the part between wall vortices decrease with increasing downstream distance; 3) the tangential velocity gradients increase with increasing cross-wind velocity.

References

1. Church, C. R., Snow, J.T. and Dessens, J., Intense atmospheric vortices associated with a 1000 MW fire, *Bull. Amer. Met. Soc.*, 61, 682-694, **1980**.
2. Terada, T., Whirlwinds on September 1-2, 1923, Report of committee on the earthquake prevention, 100, 185-27, **1925**.
3. Fujiwara, S., Report of the investigation of the Kanto Earthquake of 1923. Meteorology, 1-161, **1924**.
4. Soma, S., Study on the fire-tornado at the former site of the Hifukusho (the army clothing depot), *J. geography*, 84, 204-217, **1975**.
5. Soma, S. and Saito, K., Reconstruction of fire whirls using scale models, *Combust. Flame,* 86, 269-284, **1991**.
6. Mitsuta, Y. and Monji, N., Fire-induced vortices, *Disaster Prevention Research Institute annuals. Kyoto univ.*, 25, B-1, 255-271, **1982**.
7. Margason R. J., Fifty Years of Jet in Cross Flow Research, *Proceedings of AGARD Meetings*, CP-534, 1-1 - 1-41, **1993**.
8. Fric, T. F. and Roshko, A., Vortical structure in the wake of a transverse jet, *J. Fluid Mech.*, 279, 1-47, **1994**.
9. Kelso, R. M., Lim, T. T. and Perry, A. E., An experimental study of round jets in cross-flow, *J. Fluid Mech.*, 306, 111-144, **1996**.
10. Dessens, J., Man-made tornadoes. *Nature*, 193, 13-14, **1962**.
11. Graham, H. E., Fire whirlwinds, *Amer. Met. Soc.* , 36, 99-103, **1955**.
12. Emori, R. I. and Saito, K., Model experiment of hazardous forest fire whirl, *Fire Tech.*, 18, 319-327, **1982**.
13. Wu, J. M., Vakili, A. D., and Yu, F.M., Investigation of the Interacting Flow of Nonsymmetric Jets in Crossflow, *AIAA J.* , 940-947, Vol.26, No.8, **1988**.
14. Botros, P. E. and Brzustowski, T. A., An experimental and theoretical study of the turbulent diffusion flame in cross-flow., *17th Symp. Combustion*, 389-398, **1978**.
15. Kamotani, Y. and Greber, I., Experiments on a turbulent jet in a cross flow, *AIAA J.*, 10, 1425-1429, **1972**.
16. Savory, E., Toy, N. and Ahmed, S., Experimental study of a plume in a crossflow, *J. Wind Eng. and Industrial Aerodynamics*, 60, 195-209, **1996**.